Top Catal (2016) 59:1438–1457
DOI 10.1007/s11244-016-0653-4

ORIGINAL PAPER

H_2 Production via Ammonia Decomposition Using Non-Noble Metal Catalysts: A Review

T. E. Bell[1] · **L. Torrente-Murciano**[1]

Published online: 26 July 2016

Abstract The wide-spread implementation of the so-called hydrogen economy is currently partially limited by an economically feasible way of storing hydrogen. In this context, ammonia has been commonly presented as a viable option for chemical storage due its high hydrogen content (17.6 wt%). However, its use as an energy carrier requires the development of catalytic systems capable of releasing hydrogen at adequate rates and conditions. At the moment, the most active catalytic systems for the decomposition of ammonia are based on ruthenium, however its cost and scarcity inhibit the wide scale use of these catalysts. This issue has triggered research on the development of alternative catalysts based on more sustainable systems using more readily available, non-noble metals mainly iron, cobalt and nickel as well as a series of transition metal carbides and nitrides and bimetallic systems, which are reviewed herein. There have been some promising cobalt- and nickel-based catalysts reported for the decomposition of ammonia but metal dispersion needs to be increased in order to become more attractive candidates. Conversely, there seems to be less scope for improvement of iron-based catalysts and metal carbides and nitrides. The area with the most potential for improvement is with bimetallic catalysts, particularly those consisting of cobalt and molybdenum.

Keywords Hydrogen storage · Sustainable catalysts · Ammonia decomposition · Cobalt · Iron · Nickel · Bimetallic

✉ L. Torrente-Murciano
lt416@cam.ac.uk

[1] Department of Chemical Engineering and Biotechnology, University of Cambridge, Pembroke Street, Cambridge CB2 3RA, UK

1 Introduction

It is generally accepted, not only by the scientific community but also by politicians, environmentalists and the general public that our current energy system based on fossil fuels cannot sustain the predicted trends in the growth of the population and the increase of energy demand per capita without damaging our environment and contributing to global warming [1]. These complex and interrelated global challenges are continuously motivating the search for new energy sources and vectors. In this framework, hydrogen is often presented as an attractive alternative. Hydrogen is a clean energy vector for portable applications using fuel cells, with water as the only by-product of combustion [2]. It can be produced sustainably via water splitting using surplus renewable energy to balance the grid demands. However, the potential of the called "hydrogen economy" is currently limited by the inability to store hydrogen in a safe and economical manner with a sufficiently high density without using controversial high pressures [3].

In 2015, the US Department of Energy (DoE) released targets for the physical storage of hydrogen. These include: high storage capacity (9 wt% hydrogen content, 81 g L^{-1} volumetric capacity as shown in Fig. 1), low cost, operational temperatures below 60 °C, rapid system filling and inert and non-toxic materials [4, 5]. Hydrogen can be stored in high pressure cylinders, although there is an inherent cost associated to this technique as well as the risk of explosion with poor public acceptance. Indeed, the safety of the storage and transportation methods of hydrogen is a concern which is currently slowing the widespread uptake of the existing hydrogen fuel cell technologies. Furthermore, as shown in Fig. 1 pressurised hydrogen at 350 bar and 700 bar does not meet the 2015

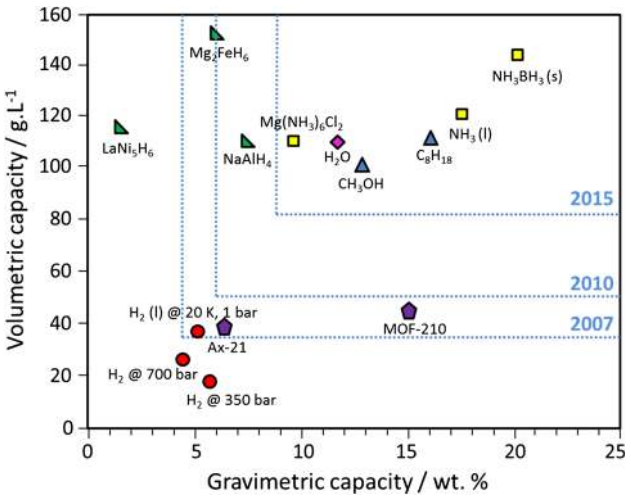

Fig. 1 Volumetric versus gravimetric hydrogen density for various hydrogen storage compounds. The US Department of Energy targets for hydrogen storage are shown by *dashed lines* [5–10]. *Circle* hydrogen under different conditions, *triangle* hydrocarbons, *pentagon* materials for H_2 physisorption, *right angle triangle* metal hydrides, *diamond* water, *square* ammonia and related compounds

US DoE targets in terms of volumetric and gravimetric capacity.

A more attractive way of physically storing hydrogen is by its adsorption in porous materials such as zeolites, porous carbons, microporous polymers and metal organic frameworks (MOFs) [1, 5, 6]. In the last decade, there has been a great progress in this area with the development of MOFs, achieving the gravimetric targets of the US DoE. However, these materials are currently unable to uptake and release hydrogen at the demanded rates and in most cases, the adsorption processes require very low operational temperatures (e.g. −196 °C for 7.5 wt% H_2 adsorption on MOF-177) [1, 7].

Aside from physical methods, hydrogen can also be chemically stored in molecules such as methanol, methane, metal amine salts (e.g. $Mg(NH_3)_6Cl_2$), ammonia and related compounds (e.g. NH_3BH_3) or in hydrides (interstitial H as in $LaNi_5H_6$ or complex hydrides such as $NaAlH_4$) [7, 10]. As shown in Fig. 1, most of these hydrogen-rich molecules meet the 2015 US DoE targets for hydrogen storage. Out of these, ammonia has highly attractive chemical and physical properties as a carbon-free hydrogen vector, containing a significantly higher amount of hydrogen than liquefied hydrogen on a volumetric and gravimetric basis [8]. Additionally, from a safety point of view, ammonia has a relatively narrow combustion range of 16–25 % in air, compared with 4–75 % for H_2 [11, 12]. Although the toxicity of ammonia may be a concern for specific uses, its strong smell is useful for identifying leaks or alternatively this issue can be completely overcome by the use of metal ammines such as $Mg(NH_3)_6Cl_2$ or $Ca(NH_3)_8Cl_2$ [7, 11]. Furthermore, ammonia can be liquefied at low pressure of 10 bar at 298 K, facilitating its transport and storage [13].

1.1 Hydrogen Production via Ammonia Decomposition

The production of CO_x-free hydrogen via ammonia decomposition (Reaction 1) for its use in a proton exchange membrane fuel cell (PEMFC) was first proposed by Green [14] in 1982. It is important to note that this is a reversible reaction, thermodynamically limited at low temperatures. Any NH_3 remaining in the inlet stream to the PEMFC can potentially damage the Nafion^{TM} polymer membrane so a robust separation method is required for the pre-purification of hydrogen [7]. Alternatively, an attractive process is the use of membrane reactor as reported [15, 16].

$$2NH_3(g) \rightleftarrows 3H_2(g) + N_2(g) \quad (1)$$

Catalytic cracking or decomposition of ammonia is the reverse reaction of the Haber–Bosch synthesis of ammonia, one of the most extensively researched processes over the past 150 years [17]. Ammonia is commonly used in the production of fertilisers and household cleaning products and therefore has well-established protocols for its handling and usage and a safe existing transportation and distribution network [12]. In order to benefit from the absence of CO_x emissions associated to hydrogen as a fuel in PEMFC, the whole process, from production to consumption needs to be CO_x free [10]. At the moment, ammonia is produced globally at a large scale of over 100 million tonnes annually, mainly from fossil fuels but new research is demonstrating its sustainable production from heat waste and renewable electricity sources such as solar, wind, hydro or geothermal energy in combination with air and water or biomass or organic waste [10, 12].

A similar important challenge, which is the subject of this review, is the delivery of hydrogen from ammonia. The US Department of Energy has clearly indicated that the feasibility of ammonia as hydrogen storage molecule relies on its decomposition at temperatures aligned with those of the PEM fuel cell, in the range of 150–180 °C making necessary the development of catalysts active under these conditions [18]. To date, the most effective catalyst for ammonia decomposition consists of ruthenium particles supported on carbon nanotubes (CNT) due to their high conductivity (6353 $mol_{H_2}\ mol_{Ru}^{-1}h^{-1}$ at 430 °C) [2, 17]. The low temperature activity can be further improved by the addition of an electron donating promoter such as cesium (7870 $mol_{H_2}\ mol_{Ru}^{-1}h^{-1}$ at 370 °C) [3, 17, 19, 20]. Furthermore, the synergetic effect of cesium and the

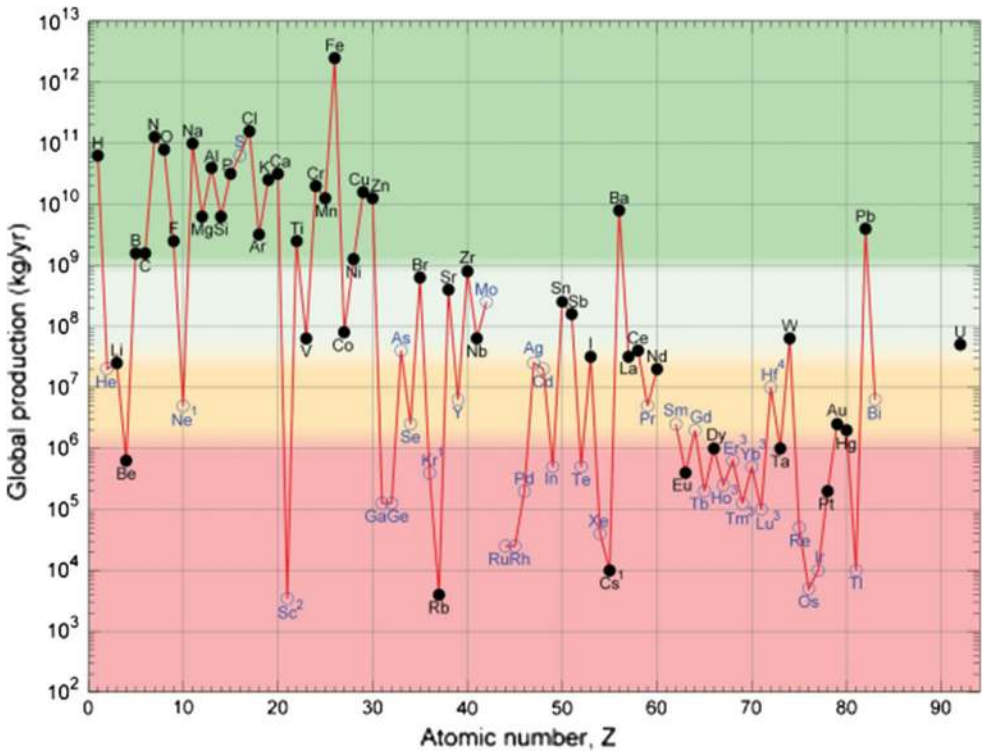

Fig. 2 Global production of elements in 2010 as a function of atomic number. Elements shown in *blue* are not obtained directly. Reproduced from Ref. [21] with permission from The Royal Society of Chemistry

graphitisation of the carbon nanotubes support on the ruthenium nanoparticles have recently enabled the decomposition of ammonia at temperatures as low as 180 °C, representing a breakthrough in the field [17].

Despite the excitement of these results, the cost and scarcity of ruthenium and cesium as shown in Fig. 2 is likely to limit the economic feasibility of the in situ production of H_2 from ammonia in PEMFC using Ru-based catalysts. Thus, the scientific community has been working on the development of alternative catalysts based on more readily available and more sustainable metals. Progress in this field to date is the focus of this review, including both non-noble monometallic (Fe, Co, Ni) and bimetallic systems (based on Fe, Co, Ni) based on elements with a high annual production (Fig. 2).

1.2 Mechanism of Ammonia Decomposition Over Heterogeneous Catalysts

In order to understand the superior activity of ruthenium-based catalysts, it is important to consider the reaction mechanism of ammonia decomposition, which is initiated by the adsorption of ammonia onto the active site surface. The adsorbed ammonia molecule undergoes successive N–H bond cleavage, releasing hydrogen atoms than can combine to form molecular hydrogen. The final step involves the recombinative desorption of nitrogen adatoms to yield molecular nitrogen [22]. Interestingly, even though the decomposition of ammonia is the reverse of the synthesis, catalyst do not necessarily exhibit the same activity in both directions due to a difference in rate limiting step as discussed in the work by Boisen et al. [23].

A study by Chellappa et al. [24], demonstrates that the kinetics of ammonia decomposition vary depending on the temperature and the concentration of ammonia. Across the temperature range of 520–690 °C with ammonia pressure from 7 to 104 MPa and high ammonia concentration, the reaction is said to be first order with respect to the ammonia concentration. Work by Ganley et al. [25] highlighted that at 580 °C, the rate limiting step depends on the metal component of the catalyst with the nitrogen desorption step rate limiting on iron and cobalt systems whereas the N–H bond scission step limits the kinetic rate on rhodium, iridium, palladium, platinum and copper. Based on their results, no distinction was made for the rate limiting step when using ruthenium and nickel based catalysts. However, irrespective of the metal, at low temperatures nitrogen desorption is rate limiting as demonstrated by Wang et al. [26] using NH_3 tracking experiments to confirm that strongly bound N adatoms limit the rate of NH_3 decomposition. Consequently the metal-N binding energy is a key parameter in the design of catalysts for the low temperature

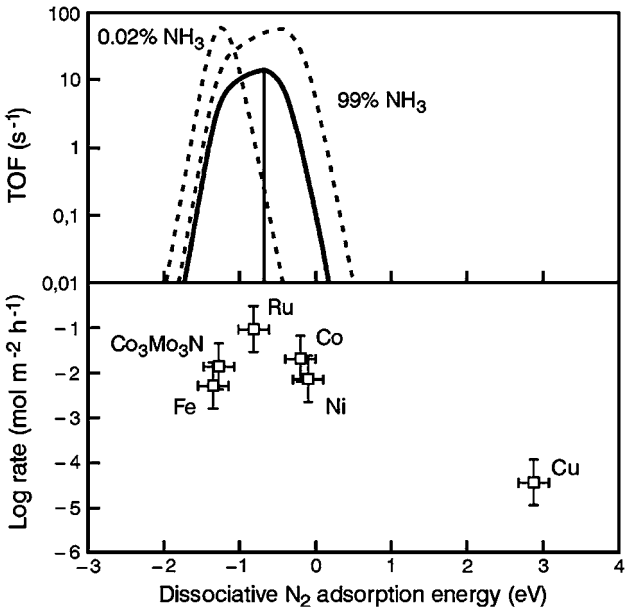

Fig. 3 *Top* Relationship between ammonia synthesis (0.02 % NH_3) and decomposition (99 % NH_3) TOF and nitrogen desorption energy. The *bold line* shows ammonia decomposition TOF with 20 % NH_3 inlet against N binding energy. The *straight line* shows the optimal value for nitrogen binding energy for 20 % ammonia gas composition. *Bottom* Experimental ammonia decomposition rate over various catalysts at 500 °C, *1 bar*, 3:1 H_2:N_2 and 20 % NH_3. Reproduced directly with permission from Boisen et al. [23]

ammonia decomposition. While the ammonia molecule needs to be adsorbed on the active metal to be activated, strongly adsorbed N adatoms would, on the other hand, poison the metal active sites. Therefore, there exists an optimum nitrogen binding energy for ammonia decomposition catalysts within the range of 544–586 kJ mol^{-1}, with the optimum activity observed at 561 kJ mol^{-1}, lower than that for ammonia synthesis catalysts [27–29].

As shown in Fig. 3, the ammonia decomposition rate of different metals and their nitrogen binding enthalpy, presents a volcano-type relationship, where ruthenium has the optimum value. This relationship constitutes one of the fundamental guidelines used in the development of alternative catalysts to the ruthenium-based ones. It is proposed that the nitrogen binding enthalpy of the ruthenium could be mimicked with stable bimetallic systems or suitable combinations of metal, promoters and support.

The two dashed lines in the top of Fig. 3 shows the difference of the reaction rate for ammonia synthesis (0.02 % NH_3) and ammonia decomposition (99 % NH_3) with respect to the metal binding energy. By comparing top and bottom of Fig. 3, it can be seen that the optimal decomposition curve is closer to Co whereas the optimal ammonia synthesis catalyst is closer to Fe in terms of nitrogen binding energy, explaining the difference in decomposition activity between Co and Fe [23].

2 Monometallic Systems

A wide range of monometallic catalytic systems have been tested for the hydrogen production via ammonia decomposition. The catalytic activity is highly dependent on the choice of metal component, the catalytic support and the potential use of promoters as well as the ammonia decomposition conditions used. Taking this into consideration, the general activity trend of monometallic systems supported on activated alumina is Ru > Ni > Rh > Co > Ir > Fe ≫ Pt > Cr > Pd > Cu ≫ Te, Se, Pb [25]. It is important to notice that the resulting activity also depends on the catalyst structure and the active site configuration in order to anchor the ammonia molecule as well as the presence of vacant sites for the release of N and H atoms [20]. Out of these metals, this review is only going to focus on those metals widely available with a focus on iron, cobalt and nickel. Some other ammonia decomposition catalysts such as transition metal carbide and nitride systems will also be considered in this section.

It is important to mention that transition metal catalysts are reported to be deactivated by sulphur impurities, resulting in the need for a pre-desulphurisation step if the ammonia feed contains sulphur. Alternatively, research has also focused on the development of sustainable catalysts that are not prone to sulphur poisoning such as the red mud catalyst reported by Uemiya et al. [30], which was believed to be resistant to sulphur poisoning due to the presence of FeC_x.

Recent work by Wang et al. [31] studied the synergy between plasma and Fe, Co and Ni catalysts for ammonia decomposition, reporting at least a five-fold improvement in catalytic activity when plasma was combined with the catalyst.

A DFT theoretical study by Duan et al. [32] calculated the activation energy and adsorption energies of reaction intermediates on Fe (110), Co (111) and Ni (111) close-packed surfaces during ammonia decomposition. The results showed that the adsorption energy of NH_3 onto Co and Ni is lower than on Fe and Fe has the highest activation energy, agreeing with experimental observations of iron-based catalysts generally having the lowest activity compared to cobalt- and nickel-based catalysts.

2.1 Iron-Based Catalysts

Iron-based catalysts are an extensively studied monometallic system for ammonia decomposition, due to its industrial use in the ammonia synthesis reaction. In this context, it is important to note that the most popular commercial catalysts for the large-scale production of ammonia are based on iron promoted with K_2O, CaO,

SiO_2, and Al_2O_3, active at temperatures above 400 °C [29]. While most of the fundamental research regarding catalyst development for ammonia decomposition is on ruthenium-based systems, the bulk price of iron is 50,000 times lower than that of ruthenium, giving rise to an obvious significant cost benefit associated to the development of effective iron-based catalysts with similar activity than ruthenium ones [18].

The relatively lower activity of iron with respect to ruthenium-based catalysts can be explained by the stronger bond enthalpy of Fe–N compared to Ru–N which can lead to the formation of surface nitrides which slows down the reaction rate and eventually deactivates the catalysts by poisoning. It is known that iron forms stable nitrides and although industrial nitridation usually takes place in the presence of ammonia at 600 °C, it has also been reported from temperatures as low as 300 °C [13]. This deactivation process is reversible at high reaction temperatures where desorption of the nitride species takes place but it is usually accompanied by sintering of iron, which deactivates the catalyst irreversibly [33].

The simultaneous occurrence of ammonia decomposition and nitridation of the iron active species was addressed by Arabczyk and Pelka [34, 35] by comparing the decomposition activity of Fe and Fe_4N. The activation energy of the latter was approximately double compared to the former highlighting that surface nitrides formation is undesirable during ammonia decomposition with a consequent reduction of the reaction rates. Detection of FeN_x as the predominant active phase on the surface was identified by a combination of high resolution TEM, elemental mapping and electron energy loss spectroscopy (EELS).

There are numerous reports focused on the kinetics of ammonia decomposition using iron-based catalysts. Generally, it is accepted that the nitrogen associative desorption is the rate limiting step [36–38]. However, several studies highlight that the limiting step varies depending on the reaction conditions (mainly temperature) due to the aforementioned formation of nitrides on the iron surface. In this context, Takezawa and Toyoshima [39] reported that while the rate limiting step at low temperatures (<479 °C) is the nitrogen desorption, at higher temperatures (>479 °C), N–H scission dictates the rate of reaction. A density functional theory (DFT) study by Lanzani and Laasonen [40] considered the mechanism of ammonia decomposition over a Fe_{55} cluster. They computed stable geometries of ammonia, N and H adsorbed to the cluster, mapping the energy landscape of the reaction mechanism. Interestingly, their results suggested that the first N–H scission step is rate limiting, contrary to the experimental kinetic studies at low temperature. They propose that the rate of decomposition of ammonia is faster with nano-sized Fe, in agreement with experimental observations as discussed in the follow subsection.

The rate of ammonia decomposition over iron-based catalysts depends on the partial pressure of ammonia and hydrogen as described by the Temkin-Pyzhev Eq. (2) [41].

$$r = k\left(\frac{p_{NH_3}^2}{p_{H_2}^3}\right)^{0.25} \quad (2)$$

The purity of the inlet ammonia stream and the presence of other gases and/or impurities can also have a beneficial or detrimental effect on the catalyst, some of them capable of altering the iron surface [41]. For example, the presence of CO_2 and H_2O was found to maintain the metallic active state of iron, leading to an enhanced activity [13].

2.1.1 *Effect of the Support on Iron-Based Systems*

A range of supported and unsupported iron based catalysts have been reported for the decomposition of ammonia, as summarised in Table 1. Unsupported catalysts typically have low surface areas and large metal particle sizes, reducing the number of exposed active sites and thus the catalytic activity. However, the unsupported systems can pose an economic advantage if they are cheap to manufacture or obtain in spite of the lower activity.

Amongst the unsupported ones, a few inexpensive iron containing materials such as ores [42] and waste products e.g. red mud [30] have been tested for ammonia decomposition. Unfortunately insufficient data was provided to enable to calculation of rate for comparison sake but nevertheless, considering the high iron content and high temperatures of the studies, it is clear that they are not exceptionally active catalysts. Nevertheless, several characteristics of the red mud present it as a viable, disposable catalyst for ammonia decomposition. Notably, since red mud is a waste product from the extraction of aluminium in the Bayer process and currently its disposal represents a problem for the mining industry, any potential uses of red mud represent not only a highly attractive economic advantage for the industry but also a sustainable solution. Additionally, red mud was reported to be resistant to poisoning by sulphur and exhibited good stability over 200 h of operation [30]. However, the composition of red mud varies depending on the bauxite source. Additionally, red mud contains a complex mixture of Fe_2O_3, SiO_2, TiO_2 and Al_2O_3, making it difficult to identify the component(s) acting as co-catalyst or promoter in the mixture. A more systematic study would be necessary to understand the role of each component on the resulting activity. The activity of a bulk iron catalyst [43] fused with small amounts (<3.3 wt%) of metal oxides (Al_2O_3, CaO and K_2O) is poor (1.14 $mol_{H_2}\ mol_{Fe}^{-1}h^{-1}$, 500 °C), which may be due to the low

Table 1 Physical properties and ammonia decomposition catalytic activity of reported iron catalysts

Details	Fe Content (wt%)	Support (Promoter)	NP size (nm)	Support S^{a}_{BET} ($m^2\ g^{-1}$)	Catalyst S^{a}_{BET} ($m^2\ g^{-1}$)	T (°C)	GHSV[b] ($cm^3\ g^{-1}_{cat}\ h^{-1}$)	Conversion (%)	Rate[c] ($mol_{H_2}\ g^{-1}_{cat}\ h^{-1}$)	Rate[c] ($mol_{H_2}\ mol^{-1}_{Fe}\ h^{-1}$)	References
Unsupported											
Red mud (Fe_2O_3, SiO_2, TiO_2, and Al_2O_3)	27.9	–	–	–	–	500	100 (h^{-1})	20	–	–	[30]
Fe containing CNT	2.8	–	10–50	–	–	500	5000	8	0.001	15	[46]
						700	5000	75.1	0.053	1057	
αFe_2O_3 – SiO_2 (Core–shell)	12.2	–	50 (Fe) 20 (Si)	–	382	500	15,000	15	0.007	127	[18]
						750	15,000	100	0.268	4908	
Nano Fe_2O_3 – SiO_2 (core–shell)	83 (2Si:10Fe)	–	–	–	34	500	30,000	24	0.041	27	[45]
Fe-CeO_2 composite	83 (5Fe:1Ce)	–	21 (Fe) 13 (Ce)	–	25	500	60	94	0.001	8.4	[47]
Limonite (α-FeOOH rich ore)	55.6	–	–	–	20	750	–	100	–	–	[48]
Goethite (FeOOH ore)	58.1	–	–	–	–	500	–	24	–	–	[42]
Fe fused with Al_2O_3, CaO, K_2O	92.7	(3.3 % Al, 3.2 % Ca, 0.8 % K)	–	–	11	500	6000	20	0.006	1.1	[43]
Fe fused with Al_2O_3, CaO, K_2O	94.8	(1.9 % Al, 2.6 % Ca, 0.7 % K)	–	–	19.3	–	–	–	–	–	[49]
Fe in Al_2O_3 matrix	95	(Al_2O_3)	10–20	–	77	500	18,000	50	0.106	125	[44]
Supported											
Fe/CNT	2.8	CNT	–	224	174	500	30,000	8	0.005	91	[50]
Fe/CMK-5	5.2	CMK-5	6	1783	1177	500	7500	26	0.012	515	[51]
Fe/C-SBA-15	5.1	Carbonised SBA-15	6	–	370	500	7500	14	0.003	152	
Fe/CNF,Mica	3.5	CNF on mica	85	–	55.6	500	6500	44	0.03	119	[52]
K-Fe/C	5.7	Graphitised C (K)	12.5	440	61 (M)	470	85,714	–	–	–	[53]
Fe/coal char	2	Coal char	10–20	–	360	750	45,000	56	–	–	[54]
Fe/Al_2O_3	1	Al_2O_3	–	–	–	–	–	–	–	–	[25]

Dash indicates data not published or insufficient data to enable calculation

[a] Surface area calculated by the BET method. Corresponds to metallic surface area when value followed by (M)

[b] Gas hourly space velocity (GHSV)

[c] Rate quoted with respect to number of moles of H_2 produced

catalyst surface area of 11 m^2/g. In fact, iron incorporated within an Al_2O_3 matrix with a higher surface area (77 m^2/g) exhibited a higher rate of hydrogen formation (125 mol_{H_2} $mol_{Fe}^{-1}h^{-1}$, 500 °C), making the case instead for the development of supported catalysts, which typically possess high surface area [44].

An alternative stabilisation strategy is the use of core–shell systems such as α-Fe_2O_3 nanoparticles surrounded by a shell of porous SiO_2 [18, 45]. The silica shell provides high thermal stability versus sintering. However, as a result of the additionally stability, higher temperatures are needed to facilitate the mass transfer diffusion of ammonia through the silica shell. As such these catalysts are only active at temperatures above 400 °C, with a promising rate of hydrogen formation of 127 mol_{H_2} $mol_{Fe}^{-1}h^{-1}$ [18] at 500 °C when only 12 wt% Fe is used. The rate per mole of iron for the core–shell catalyst containing 83 % iron is significantly lower. Nevertheless, the α-Fe_2O_3–SiO_2 core–shell catalysts are the most promising unsupported iron catalyst with respect to rate at 500 °C.

Iron nanoparticles have been supported on a range of materials including coal char, carbon nanotubes (CNT), carbon nanofibers (CNF) and structured porous carbons such as CMK-5. Research has been mainly focused on carbon materials with metal oxides being used primarily as promoters rather than supports. Carbon materials have high thermal stability and electrical conductivity, making them attractive catalyst supports [51]. Depending on the properties of the carbon support, especially its surface area and porosity, and the iron impregnation method, iron nanoparticles of different sizes have been achieved. Iron nanoparticles with average sizes of ~6 nm in diameter were stabilised on CMK-5 support (a mesoporous carbon with a dual pore network, which is formed by the templating of SBA-15 porous silica structure and subsequent removal of the template) and carbonised SBA-15 (similar to the previous support but with the SBA-15 template present) [51]. Fe/CMK-5 was found to be a more active catalyst (515 mol_{H_2} $mol_{Fe}^{-1}h^{-1}$, 500 °C) than iron supported on a carbon-SBA-15 composite (152 mol_{H_2} $mol_{Fe}^{-1}h^{-1}$, 500 °C). However, the carbonised SBA-15 support resulted in a more stable catalyst in the long term as the iron nanoparticles diffused through the carbon wall and anchored to the silica walls inhibiting their sintering.

Jedynak et al. [53] reported high TOF (0.016 s^{-1} at 400 °C, 20 % NH3) with an iron catalyst supported on graphitised carbon and linked the high activity to small particles of Fe of 13 nm (compared to 24 nm in the less active catalyst). Iron nanoparticles in the size range of 20–50 nm supported on coal chars [54] presented low activity (56 %) at high temperatures of 750 °C, even though the rate cannot be calculated, a strong link between particle size and activity can nevertheless be inferred.

From the data presented in Table 1 for supported systems, the rate of hydrogen formation (at 500 °C) is highest for the 6 nm Fe nanoparticles supported on CMK-5 [51], suggesting that small iron nanoparticles are more active for ammonia decomposition although the extent of validity of this conclusion needs to be corroborated by further work in this area. Although, this conclusion is in agreement with computational simulations of iron clusters which suggest that nano-sized particles of iron less than 10 nm in diameter increase catalytic activity [40]. By contrast, iron nanoparticles of significantly larger average sizes of 85 nm and a wide particle size distribution (40 and 160 nm) [52], achieved a superior rate (119 mol_{H_2} $mol_{Fe}^{-1}h^{-1}$ at 500 °C) to some of the catalysts with particles smaller than 10 nm.

It is worth noting that with the Fe/coal char catalyst, the formation of Fe_4N under reaction conditions was inferred by a decrease in N_2 formation rate, the presence of which could have also played a role in the lower reactivity in combination with the effect of particle size [54]. Regardless, it is clear that control of particle size by use of well-defined porous supports provides a degree of control over catalyst activity and presents an opportunity for improvement of iron based catalysts.

2.1.2 *Effect of Promoters on Iron-Based Systems*

Itoh et al. [47] synthesised Fe powders containing metal oxide components (CeO_2, Al_2O_3, SiO_2, SrO and ZrO_2). Out of them, CeO_2 and Al_2O_3 were the most effective at enhancing the catalytic activity of iron. The improvement in activity was believed to be due to the enhanced surface area and the role of the oxide as an acidic adsorbent of ammonia. Additionally, CeO_2 was also found to inhibit sintering of iron, with a 5:1 ratio of Fe:Ce showing the highest activity amongst the studied materials.

The addition of alkali metals as promoters have been reported to be effective at preventing sintering of Fe nanoparticles [55]. As an example, the addition of K_2O on iron fused with Al_2O_3 and CaO resulted in a six fold increase in ammonia decomposition rate (400 °C, 30 % NH_3) compared to the same catalysts without K_2O [49]. In the fresh promoted catalyst, K_xO_y was present both on the iron surface and on the Al_2O_3 islands found on the iron surface. Interestingly, the promoter effect of potassium varied as a function of the inlet NH_3 concentration. This was attributed to chemisorption competition on the acidic alumina sites between the more basic K_xO_y promoter and the less basic NH_3 reactant. As the inlet NH_3 concentration increases, some K_xO_y is displaced by surface diffusion onto bare iron surface and thus its effect as promoter becomes

more prevalent. No notable improvement of activity was observed with the inclusion of potassium when these catalysts were tested for ammonia synthesis [49]. An alternative explanation of the promoting effect of potassium is its effect on the resulting iron particle size. Fe/graphitised carbon catalyst promoted with a K:Fe molar ratio of 4.4:1 resulted in a fivefold increase in rate compared with the catalyst with a 1:1 ratio, which may be linked to the presence of smaller iron nanoparticles (13 nm compared with 25 nm) in the catalyst with more potassium [53].

Since both acidic (e.g. Al_2O_3) and basic (e.g. K) promoters have been reported to increase the catalytic activity of iron, the role of the promoter may lie fundamentally in the control of nanoparticle size as opposed to mediating the basicity/acidity. From the experimental works in this area, it is not clear yet if the higher activity of smaller iron particles is due to stronger promoter effects or an increase in concentration of C7 active sites, which are well known to be highly active in ammonia synthesis [53].

2.2 Cobalt-Based Catalysts

Due to the relative low cost and its nitrogen adsorption energy, cobalt has also been explored as an alternative to ruthenium for hydrogen production via the ammonia decomposition reaction. A kinetic study by Lendzion-Bielun et al. [27]. Calculated the activation energy for NH_3 decomposition to be 27 kJ mol^{-1} lower on cobalt than on iron-based catalysts. This finding can be attributed to the weaker nitrogen binding of the former compared with the latter, resulting in a superior cobalt catalyst activity, especially at low reaction temperatures.

Beyond these general aspects, the effect of the physical and chemical properties of the support (e.g. basicity and electron conductivity) [56] as well as the presence of promoters have been explored in order to understand their role and facilitate the development of active cobalt-based catalysts. Based on the current literature, the active cobalt phase for ammonia decomposition has not been clearly identified, although some reports suggest that it is metallic cobalt [27].

Consideration of the preparation and pre-treatment conditions, such as the choice of cobalt salt [57] and the calcination conditions [58], is critical as it can alter the catalysts properties, affecting the resulting ammonia decomposition activity of the catalyst. For example, work by Varisli and Kaykac [57] reported superior catalysts when synthesised from cobalt acetate compared to cobalt acetyl acetonate and cobalt nitrate. The activity and physical properties of cobalt based systems for ammonia decomposition reported in the literature are summarised in Table 2.

2.2.1 Effect of the Support on Cobalt-Based Catalysts

A series of materials have been studied as cobalt supports for the decomposition of ammonia reaction. In general, the studies reveal that the role of the support and its characteristics can be related to the cobalt particle size (nature of anchoring points), stability (depending on the metal-support interaction) and activity (e.g. electron donating properties of the support, conductivity) amongst others.

The current literature shows a range of techniques used to stabilise cobalt nanoparticles, including core–shell structures [45], incorporation within silica [55, 57] or alumina [44] matrices and ceramic [56] or carbon [20, 61, 62] supports. Carbon materials are the most studied supports due to their mechanical stability and in most cases, a good metal-support interaction with cobalt, resulting in an improved electron transfer and consequently a reduction in the nitrogen desorption energy [20]. The activity of cobalt supported on multi-walled carbon nanotubes (MWCNT) was superior to the equivalent iron and nickel catalysts with 60 % conversion at 500 °C for cobalt compared with (14.8 and 25.4 % for iron and nickel respectively) [20, 61]. The effect of the metal-support interaction on cobalt/MWCNT was studied by varying the pre-treatment temperature (230–700 °C) and gas (nitrogen and hydrogen) [62]. It was reported that pre-treatment in nitrogen resulted in higher catalytic activity compared with hydrogen and lower pre-treatment temperatures resulted in smaller nanoparticles ($\sim$6 nm) with higher dispersion, in agreement with activity trends reported by Podila et al. [58]. However, contrary to expectations, the activity of the Co/MWCNT catalyst pre-treated at 600 °C under pure nitrogen with an average Co particle size of 57.4 nm was comparable to the activity of the catalyst pre-treated at 500 °C, even though the average diameter of the cobalt nanoparticles is 9.3 nm [62]. This result is surprising as larger particles are usually less active owing to a lower surface area and a lower concentration of active sites at the surface but may be due to the effect of the nitrogen pre-treatment.

Pre-treatment of the carbon support with acid (e.g. CMK-3 treated with nitric acid [63]) has also been shown to have an effect on the control of the cobalt particle size (4–20 nm) and improve the dispersion of the cobalt nanoparticles on carbon materials [63], likely due to the creation of anchoring points however, the activity of these materials for the ammonia decomposition reaction have not yet been reported. An alternative way of achieving cobalt size control is by the incorporation in commercial cobalt nanoparticles with sizes of 4–20 nm on CNTs, which proved to be highly active with a rate of formation of 542 mol_{H_2} $mol_{Co}^{-1}h^{-1}$ at 600 °C, although a drop in rate at lower

Table 2 Physical properties and ammonia decomposition catalytic activity of reported cobalt catalysts

Details	Co Content (wt%)	Support (Promoter)	NP size (nm)	Support S^{a}_{BET} ($m^2\ g^{-1}$)	Catalyst S^{a}_{BET} ($m^2\ g^{-1}$)	T (°C)	GHSV[b] ($cm^3\ g_{cat}^{-1}\ h^{-1}$)	Conversion (%)	Rate[c] ($mol_{H_2}\ g_{cat}^{-1}\ h^{-1}$)	Rate[c] ($mol_{H_2}\ mol_{co}^{-1}\ h^{-1}$)	References
Co incorporated in Silicate	5	(Na silicate)	–	640	–	500	36,000	5	0.002	25	[55]
						600	36,000	73	0.402	4735	
Co incorporated in Silicate	17	(Na silicate)	–	–	868	500	150,000	5	0.009	31	[57]
Co_3O_4 promoted with mixed oxides	94.8	(2.9 Al, 1.6 Ca, 0.5 K, 0.23 Cr)	34	–	33 (M)	500	24,000	35	0.070	9	[59]
Co_3O_4 promoted with Ca/Al/K oxide	94	(2.8 Al, 2.4 Ca, 0.55 K)	18	–	23	500	24,000	84	0.400	50	[60]
Co-SiO_2 core–shell	83	–	–	–	–	500	30,000	15	0.016	10	[45]
Co in Al_2O_3 matrix	95	(Al_2O_3)	10–20	–	74	500	18,000	72	0.221	274	[44]
Co/mixed oxide	5	2MgAl	170	194.5	187.4	500	6000	8	0.001	11	[56]
		2MgCe	12	101.6	76.1	500	6000	40	0.023	268	
		2MgLa	22	46.7	30.7	500	6000	48	0.033	385	
Co/MgO-La_2O_3	5	MgO-La_2O_3	2.5	42	33	500	6000	60	0.051	602	[58]
Co containing CNT	4.1	–	4–20	–	–	500	5000	8	0.001	11	[46]
						600	5000	60	0.038	542	
Co/MWCNT	5	MWCNT	4.3	169.3	–	500	6000 (h^{-1})	60	–	–	[20, 61]
Co/MWCNT	10	MWCNT	57.4	–	0.2 (M)	500	6000 (h^{-1})	74.6	–	–	[62]
Co/Al_2O_3	1	Al_2O_3	–	–	–	–	–	–	–	–	[25]

Dash indicates data not published or insufficient data to enable calculation

[a] Surface area calculated by the BET method. Corresponds to metallic surface area when value followed by (M)

[b] Gas hourly space velocity (GHSV). If units differ and could not be converted, they are shown in brackets

[c] Rate quoted with respect to number of moles of H_2 produced

temperatures was observed (11 mol_{H_2} $mol_{Co}^{-1}h^{-1}$ at 500 °C) [46].

The resulting cobalt particle size can alternatively be controlled by carefully selecting a support material with appropriate and beneficial physical properties. In general, the higher the surface area of the support, the higher the metal dispersion that can be achieved. However, other characteristics of the support can override this general rule. In this context, cobalt supported on active carbons showed a lower catalytic activity than those supported on MWCNT despite of having a higher specific surface area. Nitrogen temperature programmed desorption studies show that nitrogen desorbs at lower temperatures from the Co/MWCNT catalyst than from the Co/AC, suggesting that the nitrogen binding energy is lower in the former due to superior electron conductivity of the MWCNTs respect to AC, resulting in a higher catalytic activity. A similar trend of support dependence has been reported for ruthenium catalysts which show highest activity (6353 mol_{H_2} $mol_{Ru}^{-1}h^{-1}$ at 430 °C) when supported on graphitic carbon and CNTs due to the high conductivity [17].

Due to the limited number of studies of cobalt catalysts for ammonia decomposition, it is difficult to draw concrete conclusions about the most active cobalt particle size, although in general the highest rates of conversion (at 500 °C) have been reported within the size range 10–20 nm [44, 56].

2.2.2 *Effect of Promoters on Cobalt-Based Systems*

A series of promoters have been reported in the literature to enhance the activity of cobalt active sites, especially alkali and alkaline earth metals. Co-impregnation of unsupported cobalt with calcium, aluminium and potassium oxides promoters was found to enhance the catalytic activity [59, 60]. Specifically, the promoter effect of potassium on Co/silicate catalysts increased as the quantities of KOH increased, which may be due to an increase in surface area and reduced pore diameter [55]. On the other hand, the presence of chromium and manganese on Co/mixed oxide catalyst resulted in lower activity with respect to the cobalt-only catalyst, yet no explanations were provided following this reporting [59].

Podila and co-workers [56] incorporated Mg oxide supports with Al, Ce and La oxides with a Mg:M ratio of 2:1 for use as a support of cobalt catalysts. Out of the three, the addition of LaO provided the highest activity enhancement with a rate of reaction of 385 mol_{H_2} $mol_{Co}^{-1}h^{-1}$ at 500 °C. Further studies on the Mg:La ratio, revealed an optimum 5:1 Mg:La ratio due to the stabilization of a cobalt average particle size of 15.6 nm and a high basicity of the support. There is a direct link between particle size and activity in this case, with the inactive MgAl supported catalyst possessing large cobalt nanoparticles of 170 nm whereas significantly smaller (<20 nm) cobalt nanoparticles are stabilised in the presence of lanthanum and cerium oxides, both of which yield highly active catalysts. Pre-treatment of the $MgO\text{-}La_2O_3$ support with nitrogen has been shown to yield the most active catalyst due to a modification of catalyst basicity and morphology [58] As shown in Table 2, for 5 wt% Co supported on $MgO\text{-}La_2O_3$, the rate of hydrogen formation at 500 °C increases from 385 to 602 mol_{H_2} $mol_{Co}^{-1}h^{-1}$ due to calcination of the support in air [56] and nitrogen [58] respectively. However, it is worth noting that the ratio of Mg:La is 2 in the former [56] and 3 in the latter [58] which may also contribute to the improvement in activity.

Ceria and barium have been studied as promoters for unsupported cobalt catalysts for ammonia synthesis. It was observed that addition of ceria inhibited the sintering of the cobalt particles due to the stabilisation of the hexagonal close-packed (HCP) phase of Co_3O_4 under the reaction conditions, while the addition of barium led to heat resistivity at 600 °C over 160 h [64], phenomena that can be pertinent to the development of ammonia decomposition catalysts based on cobalt.

A range of oxides materials such as Al, Ce, La, K, Mn and Cr have been studied as promoters [44, 56, 59] for cobalt based catalysts for ammonia decomposition, with the most notable enhancement in activity by lanthanum. The limited literature within this domain suggests that there is scope for further improvement of cobalt systems using novel promoter elements or methods. Although it is worth noting that the use of ceramics as promoters (or equally as supports) does present a possibility of the formation of inactive, irreducible mixed oxides such as cobalt silicate in the Co/SiO_2 catalyst [20], resulting in lower activities, identifying an area for further development of these catalysts.

2.3 Nickel-Based Catalysts

Another attractive alternative from the economic and availability points of view to substitute ruthenium on ammonia decomposition catalysts is nickel. However, nickel's high structure sensitivity, formation of irreducible Ni compounds and strong binding of hydrogen to the nickel active sites are some of the issues where further research is required for the development of an active catalyst containing highly disperse, homogeneous Ni particles [65, 66].

Computational studies of the ammonia decomposition reaction on nickel-based catalysts confirmed that similarly to the iron and cobalt catalysts, the energy of the associative desorption of nitrogen is higher than the N–H scission

step [67]. This is in agreement with the experimental kinetic studies that suggest that nitrogen recombination is the rate limiting step. Indeed, Ertl et al. [68] calculated the activation energy of ammonia decomposition over a clean Ni surface to be 197 kJ mol^{-1}. This value is similar to the energy of nitrogen desorption, confirming that the associative nitrogen desorption is the rate limiting step for nickel-based catalysts.

Temperature programmed reduction and in situ XRD have been used to identify the active phase of nickel to be the metallic form, Ni^0 [70]. It is generally accepted that the key effect of the nickel particle size is on its activity for the ammonia decomposition reaction. Figure 4 shows the relationship between nanosized nickel particles and their turn-over frequency (TOF). Only Ni^0 particles with average sizes below 2.9 nm showed considerable activity, with 2.3 nm its optimum value. Interestingly, this particle size falls into the range where the presence of B5 sites, a particular configuration of 5 atoms, is maximised as speculated by several authors [66, 69] although without experimental verification. It is important to mention here that this specific B5 sites are well known to be related to the high activity of ruthenium nanoparticles with sizes between 3–5 nm [71].

A study by Zhang et al. [69] revealed the strong effect of not only the size but also the structure on the catalytic activity of the nickel-based catalysts. Indeed, this relationship between activity and structure has been confirmed by the difference of ammonia adsorption energy between Ni (110) and Ni (111) surfaces [13]. In addition, the nitrogen desorption energy on the stepped (211) nickel surface is higher than on a close packed (111) terrace surface and in the former case, strongly adsorbed nitrogen can block up to two-thirds of the active stepped sites. Simulations studies of the ammonia decomposition reaction on nickel-based catalysts show that surfaces with too many or too few stepped sites are likely to show low activity. The nature and concentration of these stepped active sites can be controlled by varying the particle size as discussed above.

The nickel catalyst preparation method is also known to influence the catalytic activity, with co-precipitation and adsorption methods reportedly yielding more active catalysts than impregnation techniques, due to the difference in resulting nickel particle size and dispersion [65, 66, 69]. Not only the choice of method is important, but also the conditions used during the chosen procedure. For example, in the deposition–precipitation method with silica as a support, the type of Ni^{2+} phase deposited on the surface depends on the synthesis time as well as the surface area of the silica. Longer synthesis times results in increased formation of phyllosilicate which is linked to a decrease in surface and pore volume [72]. Li et al. [66] found that by using the template ion exchange method, the nanoparticles formed were predominantly on the internal walls of the support and were too small to contain a high concentration of active sites, although the exact size of these particles was not reported.

Another parameter affecting the reactivity of nickel is its loading as it can affect not only its particle size but also the nickel phase formed. In this context, Fig. 5 shows the effect of nickel loading supported on alumina via impregnation. At low loading, a high coverage of Ni atoms is formed but mainly as α-NiO. This phase is easily reduced but it also has a weak interaction with the support, making it susceptible to sintering. Higher nickel loadings resulted in the formation of γ-Ni aluminate in the spinel phase which requires reduction temperatures in excess of 800 °C but this high temperature would ultimately lead to a reduction of surface area and consequently activity [65].

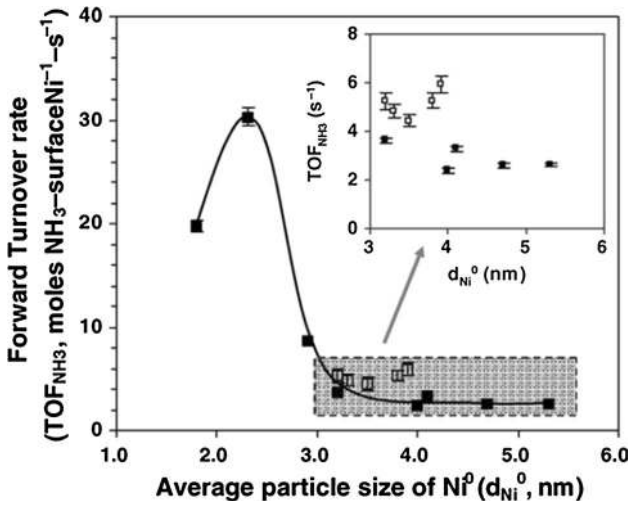

Fig. 4 Relationship between activity measured as forward TOF and average Ni^0 particle size where *solid and hollow squares* are Ni/Al_2O_3 and Ni/–La–Al_2O_3 respectively. The data highlighted in the *grey* shaded area is expanded in the *inset* graph. Directly reproduced with permission from Zhang et al. [69]

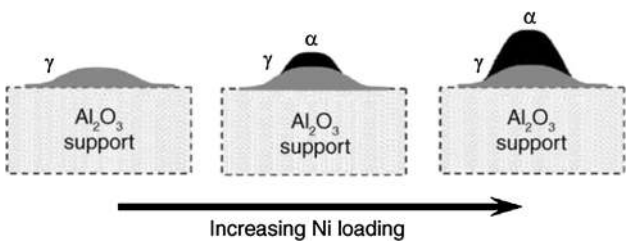

Fig. 5 Schematic of interaction of Ni with alumina support with increased Ni loading synthesised by impregnation. Directly reproduced with permission from Zhang et al. [65]

2.3.1 Effect of the Support on Nickel-Based Catalysts

The effect of the physical and chemical properties of the support are key in determining the reactivity of nickel catalysts on the ammonia decomposition reaction, mainly due their effect on the particle size and metal-support interaction discussed above. As shown in Table 3, the majority of nickel based catalysts tested for ammonia decomposition are based on ceramic supports, predominantly SiO_2 and Al_2O_3, with significantly fewer studies using carbon based supports.

Based on the current literature, carbon supports appear to be ineffective for nickel based catalysts as shown by the very low or negligible conversion at 500 °C [50, 78]. However, functionalising the multi-walled CNT (MWCNT) support with –COOH [78], resulted in an improvement in activity. The authors suggest that the increased activity may be due to nickel anchoring points created by the –COOH groups, but their presence had negligible effect on the nickel particle size, phase composition and nickel reducibility [78].

On the other hand, the use of SiO_2 and Al_2O_3 as supports has resulted in highly active of nickel catalysts. In particular, a high rate of 578 mol_{H_2} $mol_{Ni}^{-1}h^{-1}$ at 500 °C was achieved with mesoporous SBA-15 support for nickel [72] closely rivalled by the use of Al_2O_3 (496 mol_{H_2} $mol_{Ni}^{-1}h^{-1}$, 500 °C) [75]. Two highly active Ni/Al_2O_3 catalysts [65, 75] possess similar sized average nickel particles of 3.5–3.9 nm, however this size is larger than the optimal, average 2.3 nm size reported by Zhang et al. [69]. Regardless, the ability of ceramic supports to stabilise small nickel nanoparticles is promising and may play a crucial in the development of these active Ni/ceramic systems in future.

Alumina has also been shown to be effective not only as a support but also as encapsulation material of high surface area nickel microfibers [74]. The large void volume and open structure of the alumina facilitated a good heat and mass transfer with a high permeability and good heat resistance, leading to a high rate of reaction of 703 mol_{H_2} $mol_{Ni}^{-1}h^{-1}$ at 600 °C with high stability over 100 h [74].

Interestingly, complete ammonia decomposition conversion was achieved with an Al_2O_3 coated monolithic nickel catalyst at temperatures 100 °C lower compared to a packed bed of the same Ni/Al_2O_3 catalyst [73]. This is likely due to the increase in exposed nickel, although this catalyst does not outperform other Ni/Al_2O_3 presented in Table 3 Nickel nanoparticles were found to be anchored to the alumina surface as opposed to blocking the mesopores of the monolith. Thus, catalysts supported on monoliths are promising in the development of cheap, efficient and robust catalysts with a lower pressure drop, making them suitable for potential mobile applications [73].

2.3.2 Effect of Promoters on Nickel-Based Catalysts

Contrary to the observations on ruthenium-, iron- and cobalt-based catalysts, the addition of alkali metals such as potassium (by using KOH precursor) does not seem to have an effect on the catalytic activity of nickel catalysts supported on silica [66]. On the other hand, the addition of transition metals clearly shows a beneficial effect on the nickel-based catalysts. In this context, the use of lanthanum as promoter of Ni/Al_2O_3 catalysts (423 mol_{H_2} $mol_{Ni}^{-1}h^{-1}$, 500 °C) [65] results not only in morphological modifications of the nickel active sites but also in electronic effects. The presence of lanthanum can alter the local arrangement of the nickel atoms to maximise the number of stepped nickel active sites. Additionally, the surface reaction between lanthanum oxide and nickel promotes an electron transfer towards the nickel active sites which facilitates the nitrogen recombinative desorption and thus increases the rate of decomposition [69]. Alternative explanations of the beneficial effect of lanthanum suggest the promotion of a more open mesoporous structure of the Al_2O_3 support and consequently an increased nickel dispersion [65].

The addition of ceria to Ni/Al_2O_3 catalysts results in a beneficial electron transfer to the active sites with high rates reported (496 mol_{H_2} $mol_{Ni}^{-1}h^{-1}$, 500 °C) [69, 75]. Indeed, the addition of 10 wt% ceria to Ni/Al_2O_3 catalysts reduces by 100 °C the temperature at which catalysts show ammonia decomposition activity [74]. The optimum Ce:Ni molar ratio is reported to be 0.1 with Ni/Al_2O_3 catalysts [74]. Increasing the Ce loading resulted in a decrease of the Ni^0 (111) diameter and an increase of the CeO_2 (111) sites, suggesting that the optimal Ce loading could inhibit the growth of Ni, allowing a degree of control on Ni particle size [75]. Remarkable catalytic activity was reported for a triple metal microsphere catalyst containing Ni, Ce and Al [70]. The precise rate of hydrogen formation cannot be deduced due to insufficient information, however based on the small mass of catalyst tested (0.05 g) and high hydrogen formation rate in terms of mol_{H_2} g_{cat}^{-1} h^{-1}, it seems that the rate is exceedingly high on a per mole of metal basis. The activity of the reported Ni–Ce–Al microsphere catalyst was higher than for the analogous bimetallic Ni–Ce and Ni–Al catalysts, suggesting a synergistic effect between Ce and Al for promoting the activity of Ni. Thus, there is scope for enhancement of Ni/Al_2O_3–Ce catalysts as well as exploring other potential promoter metals. To our knowledge, there are no reports of promoted Ni/SiO_2 catalysts, which is surprising given the high activity of these systems,

Table 3 Physical properties and ammonia decomposition catalytic activity of reported nickel catalysts

Details	Ni Content (wt%)	Support (Promoter)	NP size (nm)	Support S^{a}_{BET} ($m^2\ g^{-1}$)	Catalyst S^{a}_{BET} ($m^2\ g^{-1}$)	T (°C)	GHSV[b] ($cm^3\ g_{cat}^{-1}\ h^{-1}$)	Conversion (%)	Rate[c] ($mol_{H_2}\ g_{cat}^{-1}\ h^{-1}$)	Rate[c] ($mol_{H_2} mol_{Ni}^{-1}\ h^{-1}$)	References
Ni–SiO_2 core–shell	83	–	–	–	112	500	30,000	35	0.087	61	[45]
Ni in Al_2O_3 matrix	95	–	–	–	121	500		60	0.153	189	[44]
Ni/monolith	15	Al_2O_3 covered monolith	6	258	39.4	500	35,294	20	0.033	77	[73]
Ni/microfibre	10	Al_2O_3 (CeO_2)	25	69	–	600	22,307	100	0.467	703	[74]
Ni/Al_2O_3	43.4	Al_2O_3 (CeO_2)	3.5	181	–	500	30,000	71.9	0.367	496	[75]
Ni/Al_2O_3	2.8	Al_2O_3	2.3	–	–	540	60,000	–	–	–	[69]
Ni/Al_2O_3	37.8	Al_2O_3 (La)	3.9	–	143	500	30,000	62	0.273	423	[65]
Ni/Al_2O_3	1	Al_2O_3	–	–	–	–	–	–	–	–	[25]
Ni/SiO_2	10	SiO_2	–	–	–	600	30,000	10.5	0.008	46	[76]
Ni/SiO_2/Al_2O_3	65	SiO_2 + Al_2O_3	–	–	–	600	30,000	21.7	0.033	30	
Ni/MgO	30	MgO	–	–	–	500	15,000 (h^{-1})	30	–	–	[77]
Ni–Ce–Al–O microsphere	–	(Ni:Ce:Al:O 0.5:0.1:0.4:x)	3.6	–	149	500	18,000	88	0.330	–	[70]
Ni/SBA-15	23.4	SBA-15	–	838.5	365	500	30,000	57	0.23	578	[72]
Ni/SBA-15	7.2	SBA-15	8	762	389	500	30,000	22	0.03	248	[66]
Ni/MCM-41	7.2	MCM-41	8	991	742	500	30,000	26.9	0.045	371	
Ni/CNT	5	MWCNT-COOH	8.1	233	–	500	6000 (h^{-1})	25.4	–	–	[78]
Ni/CNT	5	SWCNT	–	380	–	500	6000 (h^{-1})	1	~0	~0	
Ni/Graphene	5	Graphene	–	750	–	500	6000 (h^{-1})	1	~0	~0	
Ni/CNT	2.9	CNT	–	224	170	500	30,000	9	0.006	116	[50]

Dash indicates data not published or insufficient data to enable calculation

[a] Surface area calculated by the BET method

[b] Gas hourly space velocity (GHSV). If units differ and could not be converted, they are shown in brackets

[c] Rate quoted with respect to number of moles of H_2 produced

presenting an attractive opportunity for further improvement.

2.4 Other Monometallic Systems

A range of other monometallic systems have been studied for the production of hydrogen from ammonia using non-noble metals including transition metal carbides (MoC_x, VC_x, WC_x and FeC_x) and nitrides (MoN_x, VN_x and WN_x), as well as zirconium oxynitride. Out of these, molybdenum nitride and tungsten carbide are the most studied in the ammonia decomposition reaction. However, it is worth noting that these catalysts are typically tested under conditions comparable to the clean-up of gasification mixtures as well as for the production of hydrogen [13]. As shown in Table 4, the conversion of these catalysts by the rates of hydrogen formation at 500 °C per mole of metal are in general disappointingly low due to the high metal content.

Molybdenum nitride (MoN_x) is considered the most active catalyst amongst the studied transition metal carbides and nitrides, with a catalytic activity comparable to that of platinum, however the rate of reaction at 500 °C is inferior (10 mol_{H_2} mol_M^{-1} h^{-1}) [82] to mesoporous WC per mole of metal (111 mol_{H_2} mol_M^{-1} h^{-1}) [13, 81]. Note the increase in rate at 500 °C from 3 to 111 mol_{H_2} mol_M^{-1} $h^{-1}$when mesoporous WC [81] is used rather than bulk WC [80], likely due to the increase in catalyst surface area from 1.5 to 138 m^2 g^{-1}. It is known that formation of metal carbides modifies the electronic structure of the tungsten atom, responsible of its activity. However, the chemical stability of WC is low, being irreversibly poisoned in the presence of CO and H_2 at temperatures in excess of 500 °C, likely due to the decomposition of the WC compound, making it impractical for use as an industrial catalyst [80]. The decomposition of WC results in the loss of carbon at the surface, which is most likely needed to electronically modify and activate tungsten for ammonia decomposition [13]. Additionally, WC exhibited an induction period which is believed to be related to the restructuring of the WC surface in the presence of ammonia [80]. For example at 500 °C (in the absence of CO and H_2) the initial reaction rate was 3 mol_{H_2} mol_M^{-1} h^{-1} but increased after 60 min the rate to 6 mol_{H_2} mol_M^{-1} h^{-1}, after which the rate remained constant for the subsequent 300 min tested [80].

MoN_x is the active compound formed during reaction in the presence of ammonia when molybdenum oxide (MoO_3) is used as fresh catalyst. The activity of MoN_x was considerably improved after ball milling of the MoO_3 catalyst due to the increase in specific surface area from 1 to 13 m^2 g^{-1} [82]. Complementary experimental and theoretical studies by Zheng et al. [83] demonstrated that the high rate of ammonia decomposition over molybdenum carbide and nitride can be attributed to the energetic sites comprising of twin boundaries, faults in stacking, steps and defect sites. Further development of the MoN_x catalyst is needed to achieve a net cost effective system compared to the ruthenium-based catalysts, especially considering that the cost of molybdenum is half of that of ruthenium, the molybdenum-based catalyst have a very low surface area (bulk systems) compared to the highly dispersed ruthenium ones. Despite this, unless higher active surface area is achieved on molybdenum-based systems, no economic advantage would be achieved versus ruthenium systems owing to the significantly lower current rate of hydrogen formation of MoN_x (10 mol_{H_2} mol_M^{-1} h^{-1}, 500 °C) [82] compared to Ru/CNT (6353 mol_{H_2} mol_M^{-1} h^{-1}, 430 °C) [3].

On a similar note, some metal amides, such as lithium amide, can decompose under heating, forming imides compounds or mixtures of imide-amide. These compounds

Table 4 Physical properties and ammonia decomposition catalytic activity of reported miscellaneous bulk monometallic catalysts

Details	NP size (nm)	Support S_{BET}^a (m^2 g^{-1})	Catalyst S_{BET}^a (m^2 g^{-1})	T (°C)	GHSV[b] (cm^3 g_{cat}^{-1} h^{-1})	Conversion (%)	Rate[c] (mol_{H_2} g_{cat}^{-1} h^{-1})	Rate[c] (mol_{H_2} mol_M^{-1} h^{-1})	References
Li_2NH	–	–	–	450	7200	90.7	0.150	4	[79]
WC	–	–	1.5	500	2400	22	0.003	3	[80]
Meso WC	–	–	138	500	1200	100	0.028	111	[81]
MoO_3 (MoN_x active)	–	–	13	500	15,000	10	0.004	10	[82]
Mo_2C	–	–	47.7	600	36,000	85	0.545	1112	[83]
Cr_2O_3	–	–	43	600	60,000	43.4	0.237	90	[84]

Dash indicates data not published or insufficient data to enable calculation

[a] Surface area calculated by the BET method

[b] Gas hourly space velocity (GHSV). If units differ and could not be converted, they are shown in brackets

[c] Rate quoted with respect to number of moles of H_2 produced

are not expected to facilitate the decomposition of ammonia although in some cases, for example the lithium imide-amide system is effective in non-stoichiometric quantities at catalysing the decomposition of ammonia [79]. Chromium oxide has also been investigated however, it exhibits low hydrogen formation rate of 90 mol_{H_2} mol_M^{-1} h^{-1} at elevated temperature of 600 °C [84]. Mo_2C on the other hand exhibits higher and more promising rates at this elevated temperature of 1112 mol_{H_2} mol_M^{-1} h^{-1}.

In general, however, the low temperature activity of these catalysts is not particularly promising with little scope for further improvement without screening and testing novel classes of compounds.

3 Bimetallic Systems

It is well established that in general, bimetallic catalysts present different chemical properties to those of their individual monometallic components, achieving synergetic effects in particular cases [85]. Consequently, the specific arrangement of atoms within the bimetallic system can alter the catalytic activity [86]. There are different types of bimetallic systems such as core–shell or alloys. If the atoms are distributed evenly both on the surface and within the core, a perfect alloy system is formed. Core–shell particles contain a core formed by one metal surrounded by a monolayer of the second metal at the surface. In these cases, unusual chemical properties can be achieved due to the ligand effect created by the interaction of the two metals and the strain effect as the monolayer metal is constrained by the lattice of the core metal. Depending on the specific distribution of the metal atoms in a bimetallic system, its properties can result in a linear combination of the properties of the individual components or present a synergetic effect [86]. In general, bimetallic nitrides show higher activity for ammonia decomposition than their respective bimetallic oxides [87].

A requirement for bimetallic systems is a high stability under reaction conditions versus segregation into monometallic particles which would alter the surface properties and thus catalytic activity [22]. Additionally, in some supported bimetallic systems, the conditions of thermal treatment or high reaction temperatures can promote the formation of less reducible oxides such as Fe–Al, Co–Al, Ni–Al and Co–Si when supported on alumina or silica, resulting in considerably lower activity [88].

Figure 6 shows the volcano-type relationship between the catalytic activity (measured as TOF) of different monometallic systems for the synthesis of ammonia and their respective nitrogen binding energy. Out of the systems investigated, ruthenium-based catalysts present an optimum value as previously discussed herein [89]. The bimetallic guidelines mentioned above, can be applied to the rational design of bimetallic systems by combining two metals with lower and higher nitrogen binding energy than ruthenium to potentially mimic the chemical properties of ruthenium.

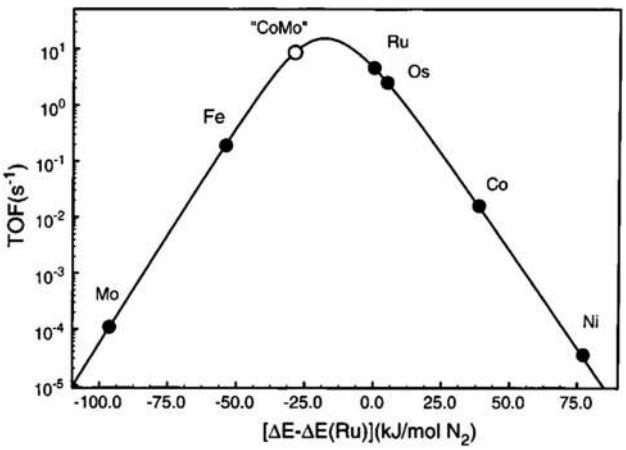

Fig. 6 Relationship between the turnover frequency (TOF) of different metals for the NH_3 synthesis reaction at 400 °C with respect to their nitrogen adsorption energy. Reprinted with permission from Jacobsen et al. [89]. Copyright (2001) American Chemical Society

A potential bimetallic system for ammonia decomposition identified by Fig. 6 is FeCo. FeCo confined on the internal surface of CNT has experimentally been shown to be an active system with a hydrogen formation rate of 4080 mol_{H_2} mol_M^{-1} h^{-1} at 600 °C [88]. The confinement of the FeCo nanoparticles within the internal CNT structure was crucial to inhibit their sintering. Additionally, a strong synergistic effect resulted not only in a high rate but also a high stability over 1000 h of operation. Elemental mapping in combination with TEM showed that the CoFe particles were alloyed and no change in the degree of alloying was found between fresh and spent catalysts. Perhaps slightly unexpected (based on the energies plotted in Fig. 6) is the reported high activity of a FeMo catalyst [90], the rate (6642 mol_{H_2} mol_M^{-1} h^{-1}) of which is superior to the aforementioned FeCo (4080 mol_{H_2} mol_M^{-1} h^{-1}) [88] catalyst at 600 °C, which may be due to the inclusion of a lanthanum promoter in the former case. Although the formation of the FeMo alloy in the fresh catalyst was verified by pXRD, under reaction conditions, the FeMo alloy is converted into the respective iron and molybdenum nitrides, but without deterioration of the activity, which suggests that these are the real active species. Additionally, the use of La_2O_3 modified Al_2O_3 as support of the FeMo particles proved to be a more effective support than Y promoted ZiO_2 due to the increased support basicity [90].

At a lower reaction temperature of 500 °C, the rate of hydrogen formation of $NiFe/Al_2O_3$ (640 mol_{H_2} mol_M^{-1} h^{-1}) [91] is superior to that of FeMo (79 mol_{H_2} mol_M^{-1} h^{-1}) [90]. In the synthesis of $NiFe/Al_2O_3$, interestingly, both incipient wetness impregnation and co-precipitation methods resulted in alloy formation with comparable activities [91]. In addition, the support was shown to influence the activity and stability of the resulting NiFe bimetallic nanoparticles. The activity of the NiFe alloy was highest when supported on Al_2O_3 and Mg–Al-Spinel compared with SiO_2, TiO_2 and ZrO_2, which may be due to a loss in surface area of the latter supports after reduction at 800 °C.

The use of first principle calculations and interpolation across the periodic table has identified CoMo as an attractive bimetallic candidate to substitute ruthenium based catalysts for the production of hydrogen from ammonia [22, 89, 98]. As shown in Fig. 6, a microkinetic simulation model identifies the CoMo combination to have a similar nitrogen binding energy to Ru. As a result, several experimental studies have focused on Co–Mo catalysts [92, 95] for ammonia decomposition, in which Co_3Mo_3N is believed to be the active species, in agreement with recent work on bulk Co–Mo catalysts by Duan et al. [93] and Podila et al. [94].

Several studies agree with the synergetic effect of the CoMo bimetallic system supported on γ-Al_2O_3 to be more active than the equivalent monometallic Co and Mo catalysts [87, 92]. The optimum Co:Mo atomic ratio varies slightly amongst studies between 7:3 [95] and 8:2 [87]. The effect of the support on the CoMo systems has also been studied by several authors with support dependant activity following the trend of γ-Al_2O_3 > MCM-41 > SiO_2 [92, 95]. In general, the activity of CoMo nitrides in ammonia decomposition increases as the surface acidity and support surface area increases. The trend in activity may also be linked to alloy particle size, with γ-Al_2O_3 and MCM-41 supports effectively stabilising small 1.8–4 nm sized particles. Unfortunately the CoMo particle size was not reported when supported on SiO_2, preventing a more in depth deduction of correlation between activity and particle size resulting from the choice of support material.

Interestingly, when the bimetallic CoMo catalyst [92] was prepared from a salt containing both metal species (i.e. $Co(en)_3MoO_4$), a higher activity and stability was achieved compared with the use of the equivalent monometallic salts. It is likely that Co and Mo have a strong interaction in the $Co(en)_3MoO_4$ salt and the higher activity can be attributed to a higher content of the Co_3Mo_3N active species. The stability of the bimetallic catalyst using $Co(en)_3MoO_4$ salt as metal precursor did not vary after 1200 h on stream, whereas the activity of the monometallic cobalt catalyst declined over this period, possibly due to the migration of cobalt to the tetrahedral γ-Al_2O_3 sites of the support forming inactive $CoAl_2O_4$. Whilst the average particle size of both the CoMo/γ-Al_2O_3 and Co/γ-Al_2O_3 catalysts was 1.8 nm, the presence of larger particles in the latter catalyst suggest that the addition of molybdenum promotes a narrower particle size distribution [92]. Further work [93] within this framework, reported significantly lower catalytic activity at 500 °C for unsupported $Co(en)_3MoO_4$ (32 mol_{H_2} mol_M^{-1} h^{-1}) compared with the supported precursor (4564 mol_{H_2} mol_M^{-1} h^{-1}) [92], likely due to the reduction in exposed active metal species. Regardless, they [93] report on the importance of calcination atmosphere and pre-nitridation temperature on the catalyst activity, with calcination in air followed by treatment at 750 °C giving the most stable and active catalyst.

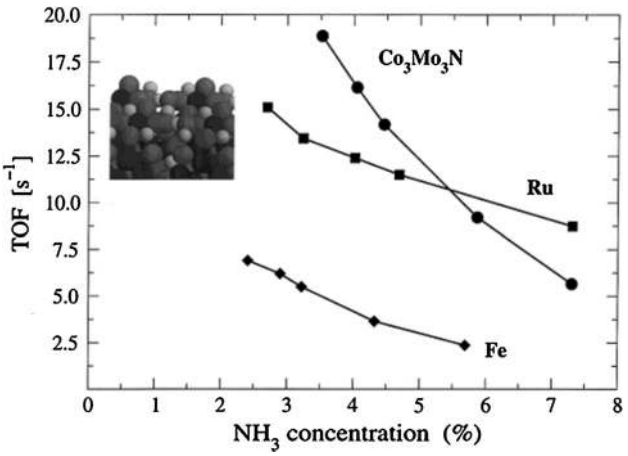

Fig. 7 Relationship between the ammonia synthesis activity of Co_3Mo_3N, Ru and Fe catalysts as a function of the ammonia concentration in the inlet stream. Reprinted with permission from Jacobsen et al. [89]. Copyright (2001) American Chemical Society

It is important to mention that work by Jacobsen et al. [89] demonstrated that the activity of CoMo nitrides in ammonia synthesis is highly dependent on the inlet concentration of ammonia in the system as shown in Fig. 7. Their work showed that, Co_3Mo_3N can present a higher activity than a ruthenium counterpart catalyst when low concentration of NH_3 below 5 % is used, although the activity dramatically decreases as the ammonia concentration increases. Whilst these results are related specifically to ammonia synthesis catalysts, this work highlights a significant limitation of Co_3Mo_3N as an ammonia decomposition catalyst. The ammonia inlet concentration is consequently an important consideration for the testing and use of Co_3Mo_3N, due to the reported poisoning at NH_3 concentrations above 5 %.

Few studies have been focussed on nickel-based bimetallic systems, amongst them, theoretical calculations of nitrogen binding energy predict a nitrogen binding energy of 582 kJ mol^{-1} for nickel supported on WC [28],

Table 5 Physical properties and ammonia decomposition catalytic activity of reported bimetallic catalysts containing at least one of iron, cobalt or nickel

Details	Combined M Content (wt%)	Support (Promoter)	NP size (nm)	Support S^{a}_{BET} (m^2 g^{-1})	T (°C)	GHSV[b] (cm^3 g^{-1}_{cat} h^{-1})	Conversion (%)	Rate[c] (mol_{H_2} g^{-1}_{cat} h^{-1})	Rate[c] (mol_{H_2} mol^{-1}_{M} h^{-1})	References
FeCo in CNT	5 (Co:Fe, 1:5)	CNT	13.7	–	600	36,000	49	0.181	4080	[88]
FeMo/ La–Al_2O_3	10 (Fe:Mo, 1:1)	La–Al_2O_3	12	90	500	46,000	8	0.007	79	[90]
					600	46,000	78	0.586	6642	
NiFe/Al_2O_3	10 (Ni:Fe, 1:4)	Al_2O_3	8–10	160	500	2400	100	0.057	640	[91]
CoMo/γ-Al_2O_3	4.8 (Co:Mo, 1:1.6)	γ-Al_2O_3	1.8	154.7	500	36,000	56	0.267	4564	[92]
$Co(en)_3MoO_4$	38.8	–	–	[5.7]	500	36,000	12	0.012	2	[93]
Co^+ Mo_2N	93 (Co:Mo 3:90)	–	14	[93]	500	6000	40	0.023	23	[94]
CoMo/MCM-41	5 (Mo:Co, 1:2.3)	MCM-41	2–4	841	500	36,000	52	0.230	–	[95]
CoMo/SiO_2	5 (Mo:Co, 1:2.3)	SiO_2	–	–	500	36,000	14	0.017	–	
NiMoN/α-Al_2O_3	10.8 (Ni:Mo, 1:1.6)	α-Al_2O_3	–	5	600	3600 (h^{-1})	79	–	–	[96]
Ni_2Mo_3N	97 (Ni: Mo 1:1.3)	–	–	[6.1]	500	21,600	29	0.043	35	[97]
Ni-Pt/Al	1–5 Ni, <1 Pt	Al_2O_3	–	158	600	–	78	–	–	[24]

Dash indicates data not published or insufficient data to enable calculation

[a] Surface area calculated by the BET method. Value in brackets for catalyst SA

[b] Gas hourly space velocity (GHSV). If units differ and could not be converted, they are shown in brackets

[c] Rate quoted with respect to number of moles of H_2 produced

which is close to the theoretical optimal value of 561 kJ mol^{-1}, however, no experimental verification is available. On the other hand, nitriding of Ni and NiMo catalysts greatly enhances the ammonia decomposition activity, although there was not a significant improvement in catalytic activity from the addition of molybdenum [96].

Whilst platinum itself is not active for ammonia decomposition, theoretical studies by Hansgen et al. [22, 86] show that when combined with nickel, iron or cobalt the binding energy increases from 418 kJ mol^{-1}, to just below the Ru (0001) binding energy of 561 kJ mol^{-1}, suggesting that platinum could be effective in enhancing the activity of nickel, iron or cobalt. However, their results show that this is only applicable for M–Pt–Pt(111) but not Pt–M–Pt(111) where M=Ni, Fe, Co and Pt are monolayers. Specifically, the stability of nickel on Pt(111) has been reported as an issue due to the migration of Ni into the first layer of Pt at 450 K [28]. Additionally, Cu, both in monometallic and bimetallic systems (in conjunction with platinum), is predicted to be inactive in this context [86].

Based on the catalytic results of bimetallic systems containing a sustainable metal substituent (iron, cobalt or nickel) it is clear from the data presented in Table 5 that CoMo is the most promising bimetallic candidate with the highest rate reported at 500 °C (e.g. CoMo/γ-Al_2O_3 4564 mol_{H_2} mol^{-1}_{M} h^{-1}) [92].

4 Outlook and Conclusions

Chemical hydrogen storage has the potential of resolving most of the current issues associated to the physical storage of hydrogen, which is currently limiting the implementation of the hydrogen economy. In this context, ammonia is presented as a highly attractive alternative due to the existing distribution network, expertise for handling and, most importantly, high hydrogen content—almost three times higher than the current storage target. The use of ammonia for on-demand hydrogen production requires the development of a new generation of catalysts based on readily available, non-noble metals as alternatives to the highly active ruthenium-based ones, which currently lead not only the highest rates but also the lowest temperature activity. It is widely accepted that the limiting step for the

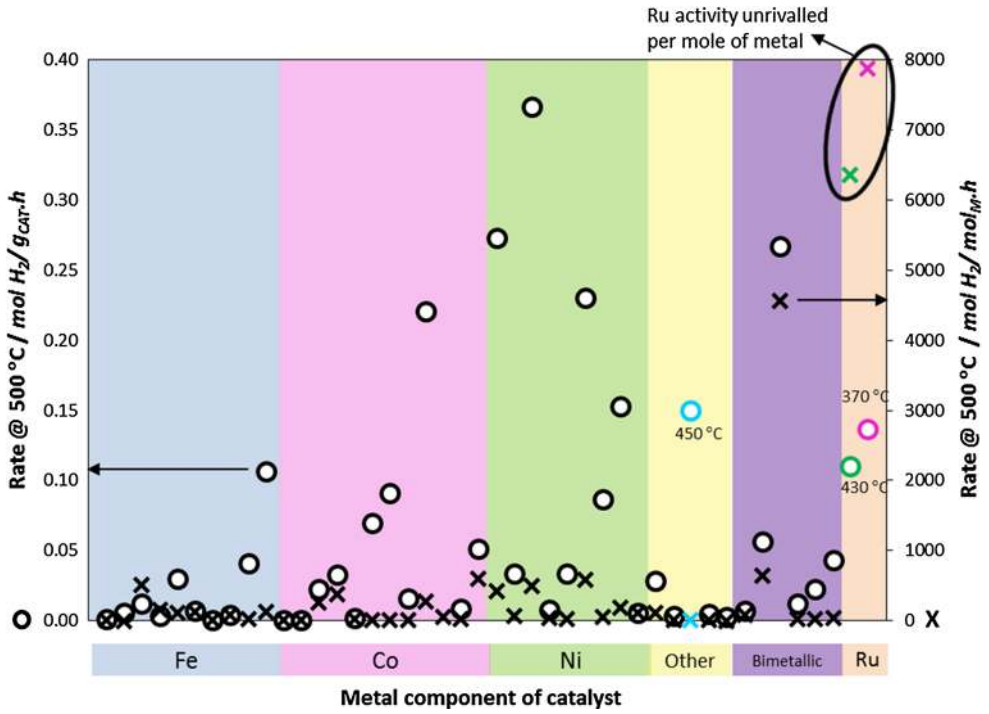

Fig. 8 Summary of hydrogen formation rate for reported iron, cobalt, nickel, other monometallic, bimetallic and ruthenium (*benchmark*) catalysts calculated for each catalyst quoted both with respect to the mass of catalyst tested (*Open circle*, *left axis*) and with respect to the number of moles of metal (*X*, *right axis*) at 500 °C or lower (if temperature differs, shown by *different coloured marker*). Refer to Tables 1, 2, 3, 4, 5 for the reference of each study and further details about the catalyst. Ruthenium benchmark catalysts are 7 wt% Ru/gCNT (*green marker*) and 7 wt% Ru/gCNT with 4 wt% Cs promoter (*pink marker*) [17]

ammonia decomposition, especially at low temperatures, is the associative desorption of nitrogen from the catalyst surface. Thus, the nitrogen binding energy of different monometallic and bimetallic systems is generally used as guideline for the rational design of novel catalysts.

Despite the low cost of iron and its industrial use in ammonia synthesis, its activity for the decomposition of ammonia is relatively low as shown in Fig. 8 due to its high nitrogen binding energy, which consequently poisons the catalyst. Based on this, there seems to be little opportunity for further development of monometallic iron catalysts although there may be potential for further improvement using acidic and basic promoters with a view to improving particle size control.

The most active cobalt catalysts tend to possess nanoparticles in the size range 10–20 and for further work the choice of support based on electronic properties and acidity/basicity is a vital consideration as well as the addition of electronic promoters. Unlike iron and cobalt, nickel supported on carbon materials is virtually inactive but the nickel activity can be enhanced using ceramic materials as support of 2–4 nm nanoparticles. While current studies focus on the high temperature activity of these systems, they show potential for the low temperature decomposition of ammonia, probably using similar promotion strategies to the ones used in ruthenium and iron systems. As shown in Fig. 8 there are a few promising reports of cobalt- and nickel-based catalysts with a high rate of hydrogen formation per gram of metal. However when these results are reported per mole of metal, none of the catalysts exhibit high activity. In addition to these metals, only lithium imide exhibits potential as an alternative to ruthenium with the reported rate at 450 °C exceeding the rate of Ru/CNT when considering the rate per gram of catalyst. However, since lithium imide is a bulk material, when the rate is quoted per mole of metal, the rate is significantly lower. Figure 8 highlights the need for increased dispersion of metallic components in order to reduce the metal content of the catalysts, resulting in improved rate per mole of metal.

Figure 8 shows that of all the catalysts reported, at 500 °C only supported Co–Mo exhibits activity close to that of Ru/CNT on a per mole of metal basis, with ruthenium based-catalysts remaining superior. Thus, we believe that the development of bimetallic catalysts, using theoretical predictions, is the most promising one. It is important to note that experimental results may disagree with theoretical predictions of proposed high activity for a particular bimetallic system but this is likely due to the difficultly of producing a pure alloy without segregation of

the metallic counterparts. As such, extensive characterisation is needed to fully understand the alloy structure. The use of metal salts containing both desired metals should also be further investigated as the improved interaction between the metals seems to lead to higher activity. In addition, the choice of catalyst preparation methods for both single metal and alloy systems is critical and it may be worthwhile moving away from wetness impregnation methods, which are often criticised for a weak metal-support interaction likely resulting in less stability and more metal segregation in bimetallic systems.

Acknowledgments The authors would like to acknowledge the UK Engineering and Physical Science Research Council (Grant Number EP/L020432/2) for funding, and SASOL UK Ltd for supporting TEB's studentship.

References

1. Eberle U, Felderhoff M, Schüth F (2009) Angew Chemie Int Ed 48:6608–6630
2. Yin SF, Xu BQ, Zhou XP, Au CT (2004) Appl Catal A Gen 277:1–9
3. Hill A, Torrente L (2014) Murciano. Int J Hydrog Energy 39:7646–7654
4. Satyapal S, Read C, Ordaz G, Thomas G (2006) 2006 Annual DOE hydrogen program merit review. In: Annual merit review and peer evaluation meeting for the hydrogen and fuel cells program. U.S. Department of Energy, Washington, DC, pp 5–6. Available at: https://www.hydrogen.energy.gov/pdfs/review06/2_storage_satyapal.pdf. Accessed 15 Jan 2016
5. Satyapal S, Petrovic J, Read C, Thomas G, Ordaz G (2007) Catal Today 120:246–256
6. David WIF (2011) Faraday Discuss 151:399
7. Klerke A, Christensen CH, Nørskov JK, Vegge T (2008) J Mater Chem 18:2304
8. Thomas G, Parks G (2006) Potential Roles of Ammonia in a Hydrogen Economy. US Department of Energy, Washington
9. Züttel A (2004) Naturwissenschaften 91:157–172
10. Lan R, Irvine JTS, Tao S (2012) Int J Hydrog Energy 37:1482–1494
11. Wojcik A, Middleton H, Damopoulos I, Van Herle J (2003) J Power Sources 118:342–348
12. Zamfirescu C, Dincer I (2009) Fuel Process Technol 90:729–737
13. Schüth F, Palkovits R, Schlögl R, Su DS (2012) Energy Environ Sci 5:6278–6289
14. Green L (1982) Int J Hydrog Energy 7:355–359
15. García-Garcíaa FR, Torrente-Murcianob L, Chadwick D, Li K (2012) J Memb Sci 405–406:30–37
16. Collins JP, Way JD (1994) J Memb Sci 96:259–274
17. Hill AK, Torrente-Murciano L (2015) Appl Catal B Environ 172–173:129–135
18. Feyen M, Weidenthaler C, Güttel R, Schlichte K, Holle U, Lu A-H, Schüth F (2011) Chemistry 17:598–605
19. Li L, Zhu ZH, Yan ZF, Lu GQ, Rintoul L (2007) Appl Catal A Gen 320:166–172
20. Zhang H, Alhamed YA, Al-Zahrani A, Daous M, Inokawa H, Kojima Y, Petrov LA (2014) Int J Hydrog Energy 39:17573–17582
21. Vesborg PCK, Jaramillo TF (2012) RSC Adv 2:7933
22. Hansgen DA, Vlachos DG, Chen JG (2010) Nat Chem 2:484–489
23. Boisen A, Dahl S, Nørskov JK, Christensen CH (2005) J Catal 230:309–312
24. Chellappa A, Fischer C, Thomson W (2002) Appl Catal A Gen 227:231–240
25. Ganley JC, Thomas FS, Seebauer EG, Masel RI (2004) Catal Lett 96:117–122
26. Wang L, Zhao Y, Liu C, Gong W, Guo H (2013) Chem Commun 49:3787–3789
27. Lendzion-Bieluń Z, Pelka R, Arabczyk W (2008) Catal. Lett 129:119–123
28. Hansgen D, Vlachos D, Chen J (2011) Surf Sci 605:2055–2060
29. Dannstadt S (2000) Ullmann's Encyclopedia of Industrial Chemistry. Wiley, Weinheim
30. Uemiya S, Uchida M, Moritomi H (2005) Mater Trans 46:2709–2712
31. Wang L, Yi Y, Zhao Y, Zhang R, Zhang J, Guo H (2015) ACS Catal 5:4167–4174
32. Duan X, Ji J, Qian G, Fan C, Zhu Y, Zhou X, Chen D, Yuan W (2012) J Mol Catal A 357:81–86
33. Zheng W (2011) Nanomaterials for Ammonia Decomposition. PhD Thesis. Universität Berlin
34. Arabczyk W, Pelka R (2008) J Phys Chem A 113:411–416
35. Pelka R, Moszyńska I, Arabczyk W (2009) Catal Lett 128:72–76
36. Löffler D, Schmidt L (1976) J Catal 44:244–258
37. Love KS, Emmett PH (1941) J Am Chem Soc 63:3297–3308
38. Logan SR, Kemball C (1960) Trans Faraday Soc 56:144
39. Takezawa N, Toyoshima I (1966) J Phys Chem 70:594–595
40. Lanzani G, Laasonen K (2010) Int J Hydrog Energy 35:6571–6577
41. Kiełbasa K, Pelka R, Arabczyk W (2010) J Phys Chem A 114:4531–4534
42. Othman NEF, Salleh HM, Purwanto H (2016) Procedia Chem 19:119–124
43. Arabczyk W, Zamlynny J (1999) Catal Lett 60:167–171
44. Gu Y-Q, Jin Z, Zhang H, Xu R-J, Zheng M-J, Guo Y-M, Song Q-S, Jia C-J (2015) J Mater Chem A 3:17172–17180
45. Yao L, Li Y, Zhao J, Ji W, Au C (2010) Catal Today 158(3):401–408
46. Zhang J, Comotti M, Schüth F (2007) Chem Commun 19:1916–1918
47. Itoh M, Masuda M, Machida K (2002) Mater Trans 43:2763–2767
48. Tsubouchi N, Hashimoto H, Ohtsuka Y (2007) Energy Fuels 21:3063–3069
49. Kowalczyk Z, Sentek J, Jodzis S, Muhler M, Hinrichsen O (1997) J Catal 169:407–414
50. Yin S, Zhang Q, Xu B, Zhu W, Ng C, Au C (2004) J Catal 224:384–396
51. Lu A-H, Nitz J-J, Comotti M, Weidenthaler C, Schlichte K, Lehmann CW, Terasaki O, Schüth F (2010) J Am Chem Soc 132:14152–14162
52. Duan X, Qian G, Zhou X, Sui Z, Chen D, Yuan W (2011) Appl Catal B Environ 101:189–196
53. Jedynak A, Kowalczyk Z, Szmigiel D, Raróg W, Zieliński J (2002) Appl Catal A Gen 237:223–226
54. Ohtsuka Y, Xu C, Kong D, Tsubouchi N (2004) Fuel 83:685–692
55. Varisli D, Kaykac NG (2012) Appl Catal B Environ 127:389–398

56. Podila S, Alhamed YA, AlZahrani AA, Petrov LA (2015) Int J Hydrog Energy 40:15411–15422
57. Varisli D, Kaykac NG (2016) Int J Hydrogen Energy 41:5955–5968
58. Podila S, Driss H, Zaman SF, Alhamed YA, AlZahrani AA, Daous MA, Petrov LA (2016) J Mol Catal A 414:130–139
59. Lendzion-Bielun Z, Narkiewicz U, Arabczyk W (2013) Materials (Basel) 6:2400–2409
60. Czekajło Ł, Lendzion-Bieluń Z (2016) Chem Eng J 289:254–260
61. Zhang H, Alhamed YA, Kojima Y, Al-Zahrani AA, Petrov LA (2013) Comptes Rendus L'Academie Bulg des Sci 66:519–524
62. Zhang H, Alhamed Y, Chu W (2013) Appl Catal A Gen 464–465:156–164
63. Zhao C, Yang Y, Wu Z, Field M, Fang X (2014) J Mater Chem A 2:19903
64. Karolewska M, Truszkiewicz E (2012) Appl Catal A Gen 445–446:280–286
65. Zhang J, Xu H, Jin X, Ge Q, Li W (2005) Appl Catal A Gen 290:87–96
66. Li X, Ji W, Zhao J, Wang S, Au C (2005) J Catal 236:181–189
67. Duan X, Qian G, Liu Y, Ji J, Zhou X, Chen D, Yuan W (2013) Fuel Process Technol 108:112–117
68. Ertl G, Rüstig J (1982) Surf Sci 119:314–318
69. Zhang J, Xu H, Li W (2005) Appl Catal A Gen 296:257–267
70. Yan H, Xu Y-J, Gu Y-Q, Li H, Wang X, Jin Z, Shi S, Si R, Jia C-J, Yan C-H (2016) J Phys Chem C 120:7685–7696
71. García-García FR, Guerrero-Ruiz A, Rodríguez-Ramos I (2009) Top Catal 52:758–764
72. Liu H, Wang H, Shen J, Sun Y, Liu Z (2008) Appl Catal A Gen 337:138–147
73. Plana C, Armenise S, Monzón A, García-Bordejé E (2010) J. Catal 2(6):484–489
74. Lu Y, Wang H, Liu Y, Xue Q, Chen L, He M (2007) Lab Chip 7:133–140
75. Zheng W, Zhang J, Ge Q, Xu H, Li W (2008) Appl Catal B Environ 80:98–105
76. Choudhary TV, Sivadinarayana C, Goodman DW (2001) Catal Lett 72:197–201
77. Takahashi A, Fujitani T (2016) J Chem Eng Japan 49:22–28
78. Alhamed YA, Zhang H, Kojima Y, Al-Zahrani AA, Hafedh D, Petrov LA (2014) Comptes Rendus L'Academie Bulg des Sci 67:519–526
79. Makepeace JW, Wood TJ, Hunter HMA, Jones MO, David WIF (2015) Chem Sci 6:3805–3815
80. Pansare SS, Goodwin JG (2008) Ind Eng Chem Res 47:4063–4070
81. Cui X, Li H, Guo L, He D, Chen H, Shi J (2008) Dalt Trans 45:6435–6440
82. Tagliazucca V, Schlichte K, Schüth F, Weidenthaler C (2013) J Catal 305:277–289
83. Zheng W, Cotter TP, Kaghazchi P, Jacob T, Frank B, Schlichte K, Zhang W, Su DS, Schüth F, Schlögl R (2013) J Am Chem Soc 135:3458–3464
84. Li L, Zhu ZH, Wang SB, Yao XD, Yan ZF (2009) J Mol Catal A 304:71–76
85. Jiang H-L, Xu Q (2011) J Mater Chem 21:13705
86. Hansgen D, Thomanek L (2011) J Chem Phys 134:174701
87. Lu CS, Li XN, Zhu YF, Liu HZ, Zhou CH (2004) Chinese Chem Lett 15:105–108
88. Zhang J, Müller J-O, Zheng W, Wang D, Su D, Schlögl R (2008) Nano Lett 8:2738–2743
89. Jacobsen C, Dahl S, Clausen BS, Bahn S, Logadottir A, Nørskov JK (2001) J Am Chem Soc 123:8404–8405
90. Lorenzut B, Montini T, Bevilacqua M, Fornasiero P (2012) Appl Catal B Environ 125:409–417
91. Simonsen S, Chakraborty D (2012) Catal A Gen 447–448:22–31
92. Ji J, Duan X, Qian G, Zhou X, Tong G, Yuan W (2014) Int J Hydrog Energy 39:12490–12498
93. Duan X, Ji J, Yan X, Qian G, Chen D, Zhou X (2016) Chem Cat Chem 8:938–945
94. Podila S, Zaman SF, Driss H, Alhamed YA, Al-Zahrani AA, Petrov LA (2016) Catal Sci Technol 6:1496–1506
95. Duan X, Qian G, Zhou X, Chen D, Yuan W (2012) Chem Eng J 207–208:103–108
96. Liang C, Li W, Wei Z, Xin Q, Li C (2000) Ind Eng Chem Res 39:3694–3697
97. Leybo DV, Baiguzhina AN, Muratov DS, Arkhipov DI, Kolesnikov EA, Levina VV, Kosova NI, Kuznetsov DV (2016) Int J Hydrog Energy 41:3854–3860
98. Jacobsen C, Dahl S, Boisen A (2002) J Catal 205:382–387